Prior-Guided Deep Interference Mitigation for FMCW Radars

Wang, Jianping; Li, Runlong; He, Yuan; Yang, Yang

DOI
10.1109/TGRS.2022.3211605

Publication date
2022

Document Version
Final published version

Published in
IEEE Transactions on Geoscience and Remote Sensing

Prior-Guided Deep Interference Mitigation for FMCW Radars

Jianping Wang, *Member, IEEE*, Runlong Li, Yuan He, *Senior Member, IEEE*, and Yang Yang, *Member, IEEE*

***Abstract*— In this article, the interference mitigation (IM) problem is tackled as a regression problem. A prior-guided deep learning (DL)-based IM approach is proposed for frequency-modulated continuous-wave (FMCW) radars. Considering the complex-valued nature of radar signals, a complex-valued convolutional neural network, which is different from the conventional real-valued counterparts, is utilized as an architecture for implementation. Meanwhile, as the desired beat signals of FMCW radars and interferences exhibit different distributions in the time–frequency domain, this prior feature is exploited as a regularization term to avoid overfitting of the learned representation. The effectiveness and accuracy of our proposed complex-valued fully convolutional network (CV-FCN)-based IM approach are verified and analyzed through both simulated and measured radar signals. Compared with the real-valued counterparts, the CV-FCN shows a better IM performance with a potential of half memory reduction in low signal-to-interference-plus-noise ratio (SINR) scenarios. The average SINR of interfered signals has been improved from −9.13 to 10.46 dB. Moreover, the CV-FCN trained using only simulated data can be directly utilized for IM in various measured radar signals and shows a superior generalization capability. Furthermore, by incorporating the prior feature, the CV-FCN trained on only 1/8 of the full data achieves comparable performance as that on the full dataset in low SINR scenarios, and the training procedure converges faster.**

***Index Terms*— Complex-valued convolutional neural network (CNN), deep learning (DL), frequency-modulated continuous wave (FMCW), interference mitigation (IM), prior feature.**

I. Introduction

FREQUENCY-modulated continuous-wave (FMCW) radars are widely used for automotive radar, vital sign detection, smart building surveillance, weather monitoring, and so on. With the rapid expansion of the applications, the mutual interference among FMCW radars as well as surrounding wireless devices becomes an increasingly severe problem, which would mask weak targets, degrade target detection and even cause ghost targets.

A number of methods have been proposed for FMCW radar interference mitigation (IM), including radar system coordination, radar system/waveform design, and signal processing approaches. Radar system coordination can operate at both the transmitter (Tx) and receiver (Rx) ends [1], which may introduce an additional communication module in the radar system. On the other hand, a new radar system/waveform can be designed (e.g., phase-coded linear-frequency-modulated continuous waveform [2]) to prevent the mutual interference. However, this method would increase the complexity of the radar system. Besides, the interference can also be suppressed in the RX end by applying signal processing approaches to received radar signals. The signal postprocessing methods do not require modification of the radar system and can be directly applied on existing FMCW radar systems. Due to this fact, in this article, we mainly focus on signal processing methods for FMCW radar IM.

The traditional signal processing approaches to IM can be further classified into four categories: 1) zeroing and reconstruction [3], [4], [5]; 2) estimation and subtraction [6], [7], [8]; 3) estimation and separation [9], [10], [11]; and 4) digital beamforming [12]. For category 1), the interference-contaminated samples in the acquired radar signals are first detected and then zeroed out to suppress interferences. To overcome the power loss of targets' signals caused by zeroing, the samples of desired targets' signals in the zeroing region can be reconstructed by the iterative fast Fourier transform (FFT)-based recovery method [3], amplitude correction (AC) [4], signal model-based extrapolation [5], and so on. However, when a very large portion of signal samples are contaminated by interferences, zeroing suppresses not only interferences but also causes severe loss of useful signals, which would significantly deteriorate the accuracy of recovered targets' signals with the reconstruction algorithms. In category 2), interferences are estimated through parameter estimation [6], or utilizing interference symmetry [7], or wavelet transform-based approach [8], and only the reconstructed interference components are subtracted from received signals. On the other hand, the desired targets' signals can be reconstructed and separated from interferences by determining the minimum of the magnitude [9]. Also, the difference of sparsity between interference and desired targets' signals is observed in the range-Doppler (RD) domain [10] and Q-factor wavelet transform domain [11], which enables

Manuscript received 4 May 2022; revised 24 August 2022; accepted 26 September 2022. Date of publication 3 October 2022; date of current version 21 October 2022. This work was supported by the National Natural Science Foundation of China under Grant 62271064 and Grant 62101378. *(Corresponding author: Yuan He.)*

Jianping Wang is with the Faculty of Electrical Engineering, Mathematics and Computer Science, Delft University of Technology, 2628 CD Delft, The Netherlands (e-mail: j.wang-4@tudelft.nl).

Runlong Li and Yuan He are with the Key Laboratory of Trustworthy Distributed Computing and Service, Beijing University of Posts and Telecommunications, Beijing 100876, China (e-mail: lirunlong@bupt.edu.cn; yuanhe@bupt.edu.cn).

Yang Yang is with the School of Electrical and Information Engineering, Tianjin University, Tianjin 300072, China (e-mail: yang_yang@tju.edu.cn).

This article has supplementary downloadable material available at https://doi.org/10.1109/TGRS.2022.3211605, provided by the authors.

Digital Object Identifier 10.1109/TGRS.2022.3211605

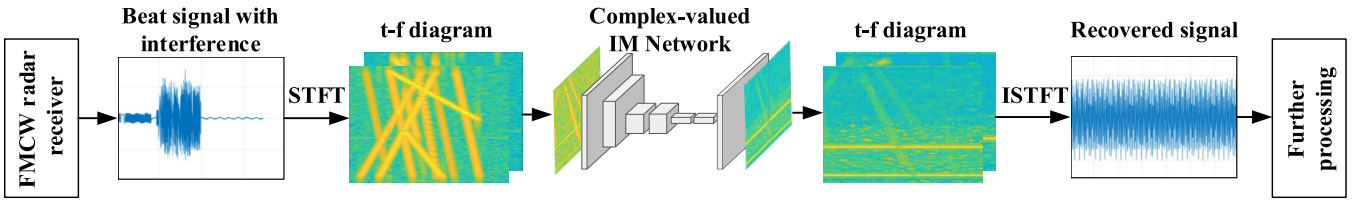

Fig. 1. Signal processing flow of our proposed approach for FMCW radar IM.

the sparsity-based nonlinear signal separation to remove the interference. Besides, in multiantenna systems, the interferences from certain directions can be mitigated by nulling through beamforming [12]. Nevertheless, the targets' signals scattered from the same directions are also suppressed.

Recent development in deep learning (DL) has shown its ability in feature extraction, and DL-based approaches are increasingly used for various signal processing problems [13], including IM for radar signals. In [14], [15], and [16], a simple convolutional neural network (CNN) is used to suppress the interference and noise by operating on the RD maps for FMCW radars. Meanwhile, more complex network structures, including fully convolutional network (FCN) [17], autoencoder [18], [19], U-Net [20], and generative adversarial network (GAN) [21], are exploited to process the frequency spectra or the RD maps of radar signals. In the time domain, recurrent neural networks (RNNs) can be implemented to process signal samples with memory ability [22], [23]. These approaches extract the feature of interferences and subtract it from received radar signals. Similarly, in [24], the CNN and residual network (ResNet) are built to detect and remove the interference components, respectively, for synthetic aperture radars (SARs). Different from the methods mentioned above, GAN can also be used to recover the missing targets' signals after interference detection and zeroing [25]. In addition, it is a good idea to combine the neural network with the traditional optimization algorithm [26], which achieves better performance and faster processing time.

Compared with the traditional signal processing methods, the DL-based approaches can extract a mapping between interfered signals and their clean references from a training dataset and show an appealing performance in complex interference scenarios even when a proper analytical signal model is unavailable. However, the lack of a large dataset of radar signals collected in various scenarios makes it hard to acquire satisfactory results for existing DL-based approaches. In addition, a small number of training data would easily lead to the overfitting problem, in which situation the features extracted by the network would be significantly affected by noise. Besides, the total parameters of the network may exceed the capacity of existing small memory-constrained radar sensors.

Generally, beat signals of FMCW radars are acquired as complex-valued samples with I/Q Rxs. The existing DL-based IM approaches all handle the real and imaginary parts of complex-valued samples as independent components with real-valued neural networks. Thus, the implicit relationship between the real and imaginary parts of radar signals was neglected, which may cause the loss of the phase information needed in further signal processing steps, such as classification and tracking. On the other hand, complex-valued CNN handles complex-valued data with standard algebraic rules of complex-valued numbers, which can achieve better performance than the real-valued counterparts [27], [28], [29]. Its potential for faster learning, easier optimization, and better generalization performance has received increasing attention in various domains [30], [31].

Considering the complex-valued nature of beat signals of FMCW radars, an IM approach based on complex-valued CNNs is proposed in this article (see Fig. 1). The proposed approach operates on the spectrogram in the time–frequency (t–f) domain. Moreover, the different t–f distribution of desired signals and interferences is exploited as a prior feature for regularization on top of the mean square error (mse) loss function, which would accelerate training and reduce the sizes of training datasets needed. The contributions of this article are summarized as follows.

1) A complex-valued FCN (CV-FCN)-based IM approach is proposed. By using complex-valued convolution and the activation function complex rectified linear unit (CReLU), a better IM performance is achieved in low signal-to-interference-plus-noise ratio (SINR) scenarios with a potential of half memory reduction compared with the real-valued counterparts.
2) A prior-guided loss function is proposed by accounting for both data consistency between labels and the recovered t–f spectra and the expected prior frequency-sparse feature of the recovered spectrogram. A hyperparameter is used for trading off between the data consistency and the expected prior feature of the recovered spectrogram. The overfitting problem can be avoided by adjusting the hyperparameter, and the networks can be trained with a smaller dataset and faster convergence.
3) The proposed IM approach can process radar signals with an arbitrary length in a sweep by splitting the short-time Fourier transform (STFT) spectrum into a combination of small matrices with certain overlap between adjacent data blocks to keep phase continuity.
4) Trained with only synthetic radar signals, the proposed approach can be directly utilized to IM for interfered radar signals collected in four dynamic scenarios. The generalization performance greatly improves by using complex-valued representation and incorporating prior feature.

The remainder of this article is organized as follows. Section II presents the signal model of interfered FMCW radars. Section III elaborates the prior-guided IM approach

based on CV-FCNs. The setups of numerical simulations for data synthesis and experimental measurements are described in Section IV. After that, the experimental results of the proposed method on the simulated and measured radar signals are presented in Sections V and VI. Finally, conclusions are drawn in Section VII.

II. Signal Modeling and Analysis

Dechirping Rx is widely used for FMCW radar systems due to its low sampling frequency requirement to analog-to-digital converters (ADCs). After dechirping, the acquired beat signals contaminated by interferences can be written as [5]

$$y(t) = s(t) + f(t) + n(t) \tag{1}$$

where $n(t)$ represents the thermal noise and measurement errors. $s(t)$ is the desired beat signals and $f(t)$ denotes the interferences, which are explicitly given by

$$s(t) = \sum_{k=1}^{N} \sigma_k \exp\left[j2\pi\left(-f_c\tau_k - K\tau_k t + \frac{1}{2}K\tau_k^2\right)\right] \tag{2}$$

$$f(t) = \mathcal{F}_{lp}\left[p^*(t)\sum_{m=1}^{M} f_m(t)\right] \tag{3}$$

where j is the imaginary unit and $0 < t < T_{\text{sw}}$ with sweep duration T_{sw}. f_c is the center frequency, K is the chirp rate of the FMCW waveform, and τ_k is the time delay of the scattered signal from the kth target relative to the transmitted one. $p^*(t)$ is the reference signal used for dechirping, $f_m(t)$ denotes the mth interference, and $\mathcal{F}_{lp}$ is the low-pass filtering (LPF) operator.

In practice, the interference component $f(t)$ could result from aggressor FMCW radars or other neighboring wireless devices. As analyzed in [5], the interferences can be generally classified into four categories: 1) interference signal with the same chirp rate as the victim FMCW sweep; 2) interference signal with different chirp rate; 3) CW interference; and 4) transient interference. For case 1), if the beat signals resulting from interferences fall in the effective bandwidth of the LPF, it, similar to real targets' signals, would result in horizontal lines along the time axis in the t–f diagram; thus, it would cause ghost targets, degrading the probability of target detection and the false alarm rate. It is difficult to mitigate this kind of interference in the time or frequency domain, and this problem may be solved by utilizing phase-modulated FMCW waveforms or IM in the space domain. Mitigation of this kind of interference is out of the scope of this article. For cases 2)–4), the interferences lead to (superposition of) inclined thick lines in the t–f diagram, which are different from the targets' signals. Therefore, without loss of generality, we consider interferences of case 2) for demonstration in this article. Note that the proposed approach is also applicable to handle interferences in cases 3) and 4).

Fig. 2 shows the t–f diagram of an interference-contaminated beat signal, where the horizontal lines along the time axis are the spectra of targets' signal components, while the inclined thick lines are the interferences. The interferences show different distributions determined by their amplitudes, chirp rates, duration times, and time delays relative to the reference signal for dechirping. Moreover, due to the positive time delay caused by wave propagation, the spectra of targets' beat signals always exist in negative frequency (if the sweep slope of the victim radar is positive and vice versa). In contrast, the spectra of interferences spread in both positive and negative frequencies in the t–f spectrum. Considering the different temporal and spectral features of targets' beat signals and interferences, it is natural to investigate possible approaches to mitigate the interferences in the t–f domain by processing, for instance, the STFT spectrum.

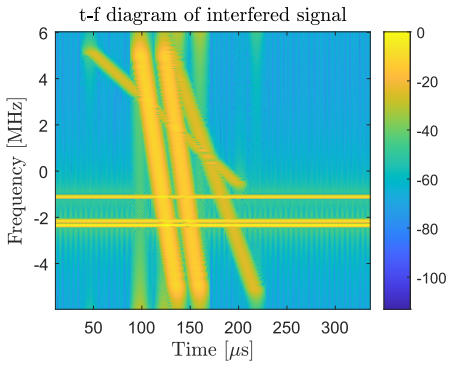

Fig. 2. t–f diagram of beat signal contaminated by mutual interferences.

Based on the different distributions of interferences and targets' beat signals in the t–f spectrum, the IM problem can be tackled as a two-step interference detection and suppression problem by using the positive–frequency spectrum to detect whether interferences exist or not. Besides, the CNN has shown its attractive performance in both interference detection and mitigation problems [24]. As a result, detecting and mitigating the interferences are addressed by exploiting an end-to-end neural network in this article.

III. Prior-Guided Deep IM

In this section, some basic modules used in the complex-valued CNN are first reviewed. Then, the CV-FCN architecture and the prior-guided loss function proposed for FMCW radar IM are introduced, followed by the detailed description of the training procedure.

A. Complex-Valued Modules

A complex-valued CNN is generally composed of various complex-valued modules, including complex-valued convolution, complex-valued activation functions, and complex batch normalization [30].

To take advantage of the existing DL platform developed for real-valued NNs (e.g., TensorFlow [32]), a complex-valued convolution can be implemented by explicitly performing real-valued convolutions among the real and imaginary parts of the related terms. Specifically, the complex-valued convolution between a complex filter $\mathbf{W} = \mathbf{A} + j\mathbf{B}$ and a complex vector $\mathbf{h} = \mathbf{x} + j\mathbf{y}$ can be expressed as

$$\mathbf{W} * \mathbf{h} = (\mathbf{A} * \mathbf{x} - \mathbf{B} * \mathbf{y}) + j(\mathbf{A} * \mathbf{y} + \mathbf{B} * \mathbf{x}) \tag{4}$$

where $\mathbf{A}$ and $\mathbf{B}$ are real-valued matrices and $\mathbf{x}$ and $\mathbf{y}$ are real-valued vectors.

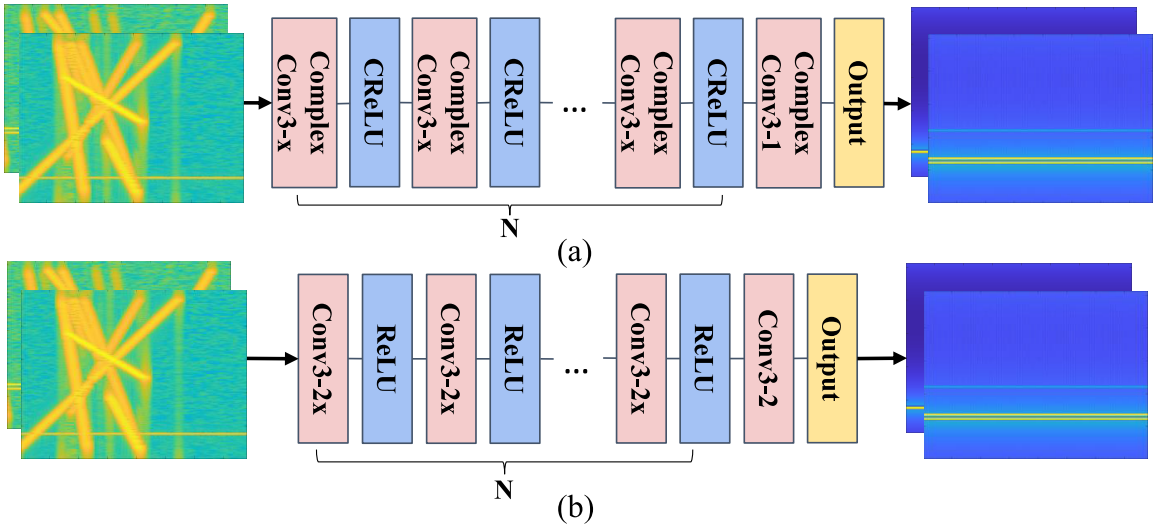

Fig. 3. (a) Proposed CV-FCN architecture. It uses the complex-valued activation function CReLU and the complex-valued convolution operation (ComplexConv), where the kernel size is 3×3 and the number of filters is **x** except for the last layer. (b) Proposed RV-FCN architecture for comparison. It uses traditional real-valued ReLU and the convolution operation (Conv), where the kernel size is 3×3 and the number of filters is $2\times$ except for the last layer.

Similar to the activation functions for real-valued CNNs, complex-valued activation functions introduce nonlinearity to complex-valued CNNs to increase their representation capabilities [30], [33], [34]. CReLU is one of the most popular activation functions used in complex-valued CNNs [30], which is implemented by using traditional real-valued ReLU on both real and imaginary parts of a complex-valued input and is expressed as

$$\text{CReLU}(z) = \text{ReLU}(\Re(z)) + j\text{ReLU}(\Im(z)) \tag{5}$$

where $\Re(x)$ and $\Im(x)$ extract the real and imaginary parts of a complex number x, respectively. Compared with other complex-valued activation functions (e.g., zReLU [34] and modReLU [33]), CReLU generally achieves the best performance in inverse problems; thus, it is utilized in this article as well.

B. Network Architecture

The IM problem can be tackled as a regression problem. Considering the complex-valued nature of FMCW radar signals in the t–f domain, a CV-FCN architecture is designed for IM with the basic complex-valued modules [see Fig. 3(a)]. The proposed CV-FCN is composed of complex convolutional layers except for the last convolutional layer, followed by the complex-valued activation function CReLU. In the last convolutional layer, only one filter is used to produce the output.

The t–f spectrum of the interfered radar signal is set as the network's input, and its counterpart of the associated reference (i.e., the clean signal) is used as the label. Since the existing DL platforms do not support the complex-valued input data, the real and imaginary parts of input samples are separated into two channels. Meanwhile, square kernels with size 3×3 are used to deal with the 2-D input samples. To keep the shape of the output t–f spectrum same as that of the input and process the edge information of each feature map, zero padding is used in the complex convolutional layers.

C. Loss Function

The mse between the outputs of the network and the related labels is generally used as a loss function in DL-based IM approaches [35]. However, the performance of the network trained with the mse as the loss function is limited by the size of the training dataset. With the increase of the network's total parameters and training iterations, the overfitting problem is inevitable, making it challenging to extract critical features. Moreover, due to the lack of labeled real interfered radar signal datasets in practice, synthetic data are commonly used for training. However, synthetic data are generally generated with analytical models derived based on certain assumptions (e.g., perfect radar system and frequency-independent scattering property of targets) for simplification, which may make the synthetic training dataset impractical to contain all the features of radar data acquired in various realistic scenarios. Consequently, the performance of the networks trained with the mse using only simulated radar signals would degrade when utilized to real data. To avoid the overfitting problem and improve the generalization of the trained network for IM in real data, explicitly incorporating the prior information to guide the network training would be of great benefit.

As shown in Section II, the interferences lead to time-varying beat frequencies after dechirping, while the beat frequencies of targets' signals are constant. The projection of the interference on the frequency axis is a line, while the projections of targets' beat signals on the frequency axis are some points. Namely, interferences and targets' beat signals show different sparsities along the frequency axis (i.e., different sparsities in the range profiles). To exploit these different prior features of interferences and targets' beat signals, we introduce the $L_{2,1}$ norm of the recovered t–f spectrogram (i.e., the output of the proposed neural network) as a regularization term

for the NN training on top of the traditional mse. Then, the complete loss function is expressed as

$$l(\mathbf{S},\tilde{\mathbf{S}}) = \left|\left|\mathbf{S}-\tilde{\mathbf{S}}\right|\right|_F^2 + \lambda\|\tilde{\mathbf{S}}\|_{2,1} \tag{6}$$

$$\|\tilde{\mathbf{S}}\|_{2,1} = \sum_{j=1}^{M}\sqrt{\sum\nolimits_{i=1}^{N}|\tilde{S}_{ij}|^2} \tag{7}$$

where $\|\mathbf{X}\|_F$ and $\|\mathbf{X}\|_{2,1}$ represent the Frobenius norm and $L_{2,1}$ norm of a matrix $\mathbf{X}$, respectively. $\tilde{\mathbf{S}} \in \mathbb{C}^{M\times N}$ is the matrix of the recovered spectrum in the t–f domain with the row and column related to the frequency and time dimensions, respectively, and $\mathbf{S} \in \mathbb{C}^{M\times N}$ is the label. $\|\mathbf{S}-\tilde{\mathbf{S}}\|_F^2$ denotes the traditional mse, and $\|\tilde{\mathbf{S}}\|_{2,1}$ characterizes the prior feature. λ is a hyperparameter used to make a tradeoff between the mse (i.e., data consistency) and the prior feature. By properly tuning λ, the trained CV-FCN fuses the prior information and the features extracted from the labeled data, which improves its generalization capability. Note that when $\lambda = 0$, the proposed loss function (6) becomes the mse.

Due to the introduced regularization term $\|\tilde{\mathbf{S}}\|_{2,1}$, the overfitting problem can be avoided as much as possible. Moreover, as the regularization term $\|\tilde{\mathbf{S}}\|_{2,1}$ provides solid expert knowledge, it boosts the convergence rate of the network training (i.e., the network can be trained with fewer iterations) and significantly reduces the size of the dataset needed for training.

D. Training Setup

Before being fed into the network, the complex-valued input samples are normalized. Specifically, the normalization method can be described as

$$\tilde{\mathbf{Y}}(m,n) = K\frac{\mathbf{Y}(m,n)}{\max_{\substack{1\le m\le M\\ 1\le n\le N}}|\mathbf{Y}(m,n)|_2} \tag{8}$$

where $\mathbf{Y}$ is the matrix of the STFT spectrum of beat signals contaminated by interferences and m and n are the row and column indices of an entry of the matrix, respectively. Due to the large amplitude difference between targets' signals and interferences in low SINR scenarios, K is a constant used to scale the normalized data to a proper range of values, which may affect the performance of trained NNs due to their nonlinearities. In this article, an empirical value $K = 10^3$ is used in the experiments. After IM with the network, the output can be rescaled to recover the t–f spectrum of a signal based on (8).

For the NN training, the complex weight initialization strategy [30] was used to initialize the parameters of complex convolutional layers, and the Adam optimizer was adopted with a fixed learning rate of 0.001 and 32 input samples per batch. The training procedure was ended after 100 epochs when good convergence was observed. Moreover, the code was implemented using Keras and TensorFlow tools, and all the models were trained on a single NVIDIA Tesla V100 graphics processing unit (GPU).

IV. Datasets

In this section, the setups of numerical simulations for data synthesis and experimental measurements are first introduced, and then, the data split approach to long-time sequence processing is presented.

TABLE I
PARAMETERS OF THE VICTIM RADAR

Parameter	Value	Parameter	Value
Center frequency	3 GHz	Moving speed	30 m/s
Duration of a sweep T_{sw}	400 μs	Window type	Hamming
Bandwidth	40 MHz	Window length	256
Chirp rate K	0.1 MHz/μs	Overlap length	255
Sampling frequency	12 MHz	FFT points	256
Maximum detection distance	8 km		

TABLE II
PARAMETERS OF THE TARGETS AND INTERFERENCES[1]

Parameter of Targets	Value	Parameter of Interferences	Value
Number	$\mathcal{U}\{0,20\}$	Number	$\mathcal{U}\{1,20\}$
Distance	$\mathcal{U}(8,8000)$ m	Amplitude[2]	$\mathcal{U}(0,3)$
Amplitude[2]	$\mathcal{U}(0,3)$	Center frequency	3 GHz
Phase	$\mathcal{U}(0,2\pi)$	Chirp rate	$\mathcal{U}(-2K,2K)$
Velocity	$\mathcal{U}(0,80)$ m/s	Duration	$\mathcal{U}(0,T_{\text{sw}})$
		Delay time	$\mathcal{U}\left(\frac{-T_{\text{sw}}}{2},\frac{T_{\text{sw}}}{2}\right)$

[1] $\mathcal{U}$ means the uniform distribution.
[2] Note that the amplitude is a relative value instead of a true value.

A. Radar Signals Synthesis

Due to the difficulties in acquiring both interfered radar echoes and their related references in practice, especially for dynamic scenarios, in this article, we use synthetic FMCW radar signals for training of the proposed neural network and then employ both synthetic and measured data for test.

For data synthesis, a victim FMCW radar with the parameters described in Table I was considered. To emulate the scenarios with various scatterers and different interferences, each parameter of targets and interfering signals was randomly chosen from a uniform distribution $\mathcal{U}[a,b]$ (or $\mathcal{U}(a,b)$) in a closed (or open) interval for continuous variables or discrete uniform distribution $\mathcal{U}\{a,b\}$, where a and b define the bounds of the interval. The detailed intervals of the values of the parameters of targets and interfering signals are shown in Table II, where K and T_{sw} refer to the chirp rate and sweep duration of the victim radar in Table I. Moreover, complex white Gaussian noise was added to synthetic signals to account for system noise and measurement errors. To characterize the interference-contaminated signals in the presence of complex white Gaussian noise, signal-to-noise ratio (SNR) and SINR are used as metrics. To be consistent with the real-world scenarios, the minimum value of SINR is set to -40 dB. The SNR ranges from -20 to 20 dB with a step size of 5 dB. For each value of SNR, the SINR must be lower or equal to it, i.e., the range of SINR varies with SNR and can be divided into 4–12 intervals with a step size of 5 dB. Then, totally 72 combinations of the value of SNR and the interval of SINR are acquired. For each combination, 60, 20, and 20 samples were randomly generated for training, validation, and testing, respectively. Consequently, we obtained a training set of 4320 samples, a validation set of 1440 samples, and a testing set of 1440 samples.

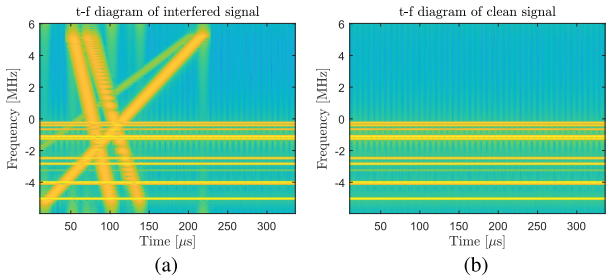

Fig. 4. $t-f$ diagrams of (a) simulated radar signal and (b) its label.

TABLE III
PARAMETERS OF THE PARSAX RADAR

Parameter	Value
Center frequency	3.315 GHz
Duration of a sweep T_{sw}	1 ms
Transmitted power	20 dBm
Bandwidth	30 MHz
Chirp rate K	30 MHz/ms
Sampling frequency	400 MHz

After synthesizing the time-domain radar signals according to the setups described above, their $t-f$ spectra are generated through the STFT by using a 256-point hamming window with a hop size of one for signal segmentation and 256-point FFT for spectrum calculation (see Table I). The $t-f$ spectra of the associated clean targets' signals are also obtained as the corresponding labels. An example is shown in Fig. 4.

B. Experimental Measurements

The experimental data used in this article were collected with the full-polarimetric PARSAX radar in TU Delft, Delft, The Netherlands, which has two orthogonally polarized transmitting channels and four receiving channels for full-polarimetric signal acquisition. The parameters of this radar are listed in Table III.

The two orthogonally polarized transmitting channels were used to simultaneously transmit different signals: horizontally polarized (H-pol) channel for a fixed FMCW signal and the vertically polarized (V-pol) channel for an arbitrary FMCW-type waveform with various chirp rates, time duration, bandwidth, and time delay relative to the beginning of the signal in the H-pol channel. The full-polarimetric signals scattered from the illuminated scene arrive at the receiving antenna at the same time. After passing through an orthomode transducer, the H-pol (i.e., HH and VH) and V-pol (i.e., HV and VV) scattered signals can be separated. However, the HH and VH (correspondingly HV and VV) signals inevitably interfere with each other at the receiving channels. As the HH (correspondingly VV) signals are generally much stronger than the VH (correspondingly HV) signals, the interference impact of HH (VV) on the VH (HV) is generally much severer. Thus, the acquired HV signals are used to construct the experimental dataset.

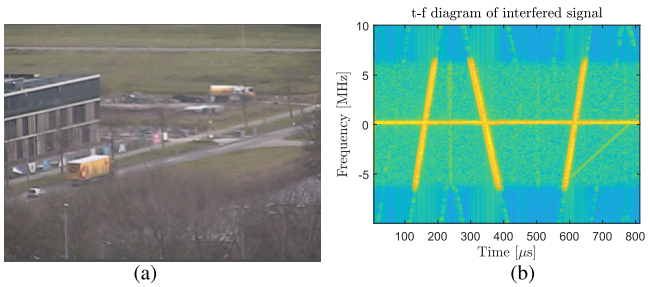

Fig. 5. Measured radar signals collected in the street with traffic flow. (a) Camera visual image. (b) $t-f$ diagram.

The radar data were measured by illuminating four scenes: an industrial chimney, a rotating wind turbine, a street with traffic flow, and A13 highway with traffic flow in Delft. In total, 500-sweep radar data were collected with various interferences for each sweep. As an example, Fig. 5 shows the street scenario at a time instant and the $t-f$ diagram of the acquired signal. As the experimental measurements were taken in wild scenarios, it is impractical to acquire the related references with our radar system, which is generally the case in practice. Thus, the associated references of the acquired experimental data are unavailable for supervised learning of the NNs. As a result, the experimental data are only used for testing of the trained neural networks in this article.

C. Data Split

In principle, the shape of the STFT spectra of radar signals is determined by the number of sampling points in a sweep and parameters of the STFT algorithm, but most CNNs can only process input samples of specific shapes. In order to process radar signals of a larger size in the $t-f$ domain, the matrix of the STFT spectrum can be split into a combination of smaller matrices before being fed into the network, which is shown in Fig. 6. The data splitting with certain overlap between adjacent data blocks aims at keeping phase continuity of the recovered signals obtained with the trained NNs. In our experiments, the overlap size of adjacent data blocks N_p is set to 8, and the shape of the input samples (i.e., $M \times M$) is 256×256.

V. SIMULATION RESULTS

In this section, the prior-guided deep IM approach is demonstrated and analyzed using synthetic FMCW radar signals. First, the performance metric used for quantitative evaluation of IM performance is presented. Then, the optimal network architecture based on the CV-FCN is obtained by grid search using the mse as the loss function, including the kernel size, number of filters in each convolutional layer, depth of the network, and additional residual connection. Next, the CV-FCNs are compared with the real-valued counterparts over a range of network depths to examine the superiority of complex-valued representation. After that, the prior-guided loss function is used to retrain the neural network optimized through the grid search method, and its effects on the training convergence and the size of the required training dataset are investigated as well.

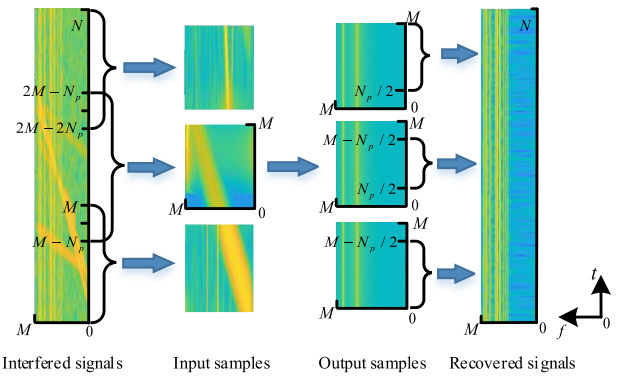

Fig. 6. Data split approach to process the t–f spectra of interfered signals with different shapes, where M and N are the sizes of the column and row related to the frequency and time dimensions, respectively, and N_p is the overlap size of adjacent data blocks along the time dimension.

Finally, the proposed approach is compared with the state-of-the-art IM approaches.

A. Performance Metrics

To quantitatively evaluate the performance of different IM methods, the SINR of a recovered radar signal relative to its clean reference and the correlation coefficient ρ were introduced, which are defined as

$$\mathrm{SINR} = 10\lg\left(\frac{||\mathbf{s}||_2^2}{||\tilde{\mathbf{s}}-\mathbf{s}||_2^2}\right) \tag{9}$$

$$\rho_{\mathbf{s},\tilde{\mathbf{s}}} = \frac{\tilde{\mathbf{s}}^H\mathbf{s}}{||\mathbf{s}||_2 \cdot ||\tilde{\mathbf{s}}||_2} \tag{10}$$

where $\tilde{\mathbf{s}}$ is the recovered signal in the time domain, $\mathbf{s}$ is the corresponding reference, and $||\mathbf{x}||_2$ denotes the L_2 norm operator of a vector $\mathbf{x}$.

The SINR can not only measure the remaining interferences and noise in the recovered signal but also evaluate possible signal distortion. Meanwhile, the correlation coefficient characterizes the similarity of the recovered signal and its clean reference in terms of waveform (via its modulus $|\rho|$) and the phase difference between them (via its argument $\angle\rho$).

Besides, we also utilized the detection rate to quantitatively evaluate the target detection performance after IM. The cell-averaging constant false alarm rate (CA-CFAR) detector and the peak grouping algorithm [36] were used for detection. The false alarm rate was fixed to 1×10^{-4}.

B. Network Architecture Optimization

To find an optimal CV-FCN architecture for the proposed IM approach and the following comparative experiments, parameter search is performed using the mse as the loss function.

Inspired by some traditional CNN architectures such as VGGNet [37] and DnCNN [38], three types of potential CV-FCN architectures, denoted as Types I–III, are considered: in Type I, the number of filters in each convolutional layer is fixed to constant except for the last layer, while in Types II and III, the number of filters is doubled (such as VGGNet) [37] or halved (such as DnCNN) in each convolutional layer, respectively. For Type I architecture, the number of filters in each convolutional layer was set to 8, 16, or 32, while the Type II (or Type III) networks with 2, 4, and 8 (or 64, 32, and 16) filters in the first layer were considered. Then, the CV-FCN networks of the three types with depth ranging from 4 to 12 and the kernels of size 3×3 and 5×5 were studied. However, due to the limited GPU memory size, the depths of networks up to 7 for Type II and 6 for Type III are considered. Thus, more Type I cases are presented. The comparison results are shown in Fig. 7, where the horizontal and vertical axes indicate the number of total parameters and the evaluation results of recovered signals.

According to Fig. 7, the CV-FCNs with Type I architecture obtain better results. For Type II, it was generally constructed with pooling layers or strides to extract high-level features. However, the pooling operation may result in signal distortion and is not utilized in the CV-FCN. Thus, the high-level features are not extracted as the VGGNet [37], and the Type II architecture did not show better results. Based on the conclusion, the CV-FCNs (Type I) with different total parameters are compared. The features of targets' beat signals and interferences in the t–f domain are relatively simple, and using a larger number of filters or a deeper network is unnecessary. The maximum average SINR is obtained using a model (Model A) with eleven layers, where each convolutional layer consists of 16 filters with kernel size 3×3 except for the last layer. Moreover, we compared the CV-FCNs (Type I) with kernels of 3×3 (Model A) and 5×5 (Model B). Although the number of total parameters in Model B triples, it leads to an average SINR of 0.31 dB lower than that of Model A. Thus, the kernel size of 3×3 is used in the following experiments.

Furthermore, residual connection was introduced to promote better backpropagation of gradient, avoiding the problems of gradient diminishing and explosion during training of a neural network [39]. To examine the effect of residual connection for complex-valued IM networks, an additional residual connection is added between the input and output of the CV-FCN (Type I), resulting in a complex-valued ResNet (CV-ResNet). According to Fig. 8, the CV-ResNet-based IM approach achieves better performance in the high SINR scenarios while performing worse in the lower SINR cases compared to the Type I CV-FCN-based ones. This can be explained as follows: in the high SINR scenarios, targets' signals are the dominant components in the radar data and have a lower dimensional structure than the mixture of noise and interferences; in such cases, it is easier for the CV-FCN (Type I) to learn the bases to annihilate targets' signals and thus with a residual connection the CV-ResNet-based IM approach eliminates the interferences and noise and outperforms the CV-FCN-based ones. However, in the low SINR scenarios, interferences are generally the largest component of the radar data and have a lower dimensional structure than the mixture of noise and targets' signals; thus, it is easier for convolutional filters of

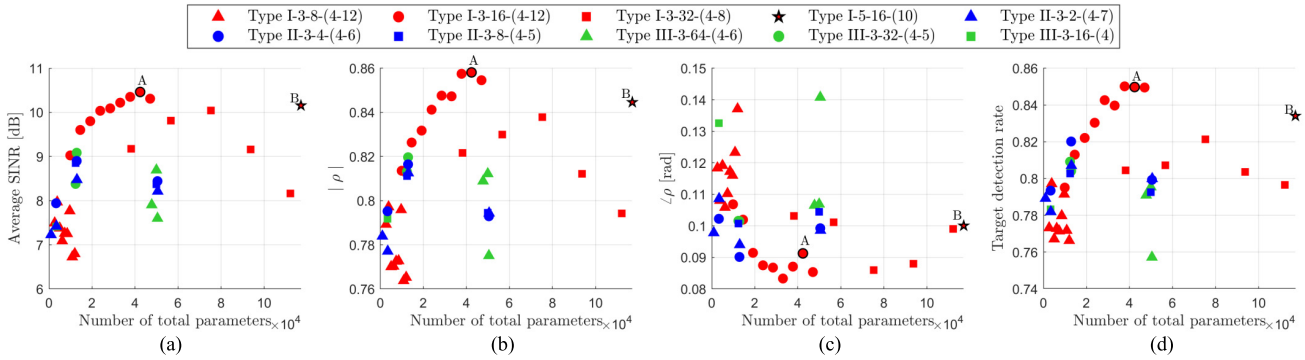

Fig. 7. Performance comparison of different network architectures based on the CV-FCN in terms of (a) average SINR, (b) modulus, and (c) phase of the correlation coefficient, and (d) target detection rate. Here, Type I-$k-m-(n_1-n_2)$ [or Type II/III-$k-m-(n_1-n_2)$] represents the network belonging to Type I (or Type II/III) with the kernels of $k \times k$, where the number of filters in each layer (or the first layer) is m, whose range of the network depth is between n_1 and n_2. In each case, the total number of parameters increases as the network deepens.

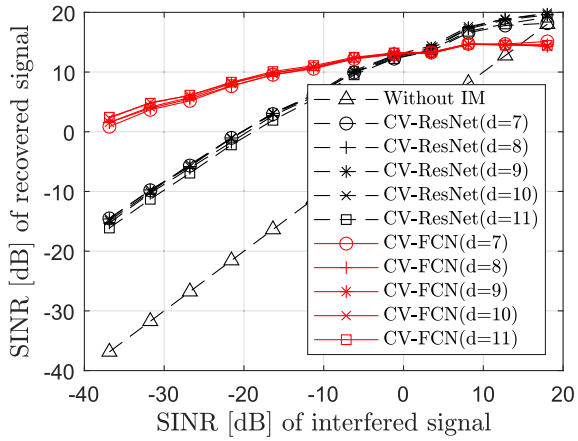

Fig. 8. Performance comparison of the CV-FCNs with CV-ResNets, where d means the number of convolutional layers in the network.

the CV-FCN to extract the features to annihilate interferences directly. As a result, the CV-FCN-based IM outperforms the CV-ResNet in the low SINR cases.

C. Performance Comparison With Real-Valued Networks

To analyze the IM performance of complex-valued networks, we compared the CV-FCNs with their real-valued counterparts over a range of network depths.

The real-valued FCN (RV-FCN) is constructed using the real-valued convolutional layer and the traditional ReLU activation function to replace their corresponding complex-valued modules. In the complex-valued networks, the number of complex filters in each layer is the number of complex feature maps, i.e., the effective number of feature maps for each of the real and imaginary parts. To obtain the same number of feature maps for fair performance comparison, the RV-FCNs were constructed in the same architecture as the corresponding CV-FCNs but with the number of filters doubled in each layer [see Fig. 3(b)].

The comparison results of the RV-FCNs and the CV-FCNs are shown in Fig. 9. One can see that the CV-FCNs of different depths show a better IM performance in the low SINR scenarios compared with their real-valued counterparts. This phenomenon is very meaningful in practice as the IM is more demanding in the low SINR scenarios. To be clear, some quantitative comparisons of the CV-FCNs and RV-FCNs in the low SINR cases are shown in Table IV. When the SINR of interfered signals is between -40 and -20 dB, all the CV-FCNs with depths varying from 6 to 12 obtain better IM performance in terms of the SINRs, modulus of the correlation coefficient, and the detection rate of the recovered signals (in bold red font) compared with the RV-FCNs. Specifically, the SINRs of the beat signals recovered by the CV-FCNs are on average 1.16 dB higher than that by the RV-FCNs. Since the detection rate depends on the accuracy of the recovered signal, the detection rates of the CV-FCNs are on average 4.46% higher than that of the RV-FCNs. However, the number of parameters of a CV-FCN is only half of that of its corresponding RV-FCN.

Next, the performance of the optimal CV-FCN with 42 370 parameters and its related optimal RV-FCN with 84 418 parameters is compared. Although the CV-FCN has 49.8% fewer parameters, it achieves almost the same performance as the RV-FCN. The optimal RV-FCN requires 1.04 MB of memory in the computer's memory, while the CN-FCN requires only 586 kB. In addition, the SINR of recovered signals has improved from 1.41 to 2.44 dB for interfered signals with the SINR from -40 to -35 dB. Thus, the CV-FCN provides a better solution to practical applications considering its parsimony requirement of hardware memory and the superior performance in suppressing strong interferences.

D. Effects of Prior-Guided Loss Function

In this section, the prior-guided loss function (6) is adopted to retrain the optimized CV-FCN (Model A) in Section V-B, and its effects on the training convergence and the size of required training dataset are investigated with different values of the hyperparameter λ.

1) Effect on Convergence Rate of Training: The synthetic dataset was used for training. Then, without loss of generality,

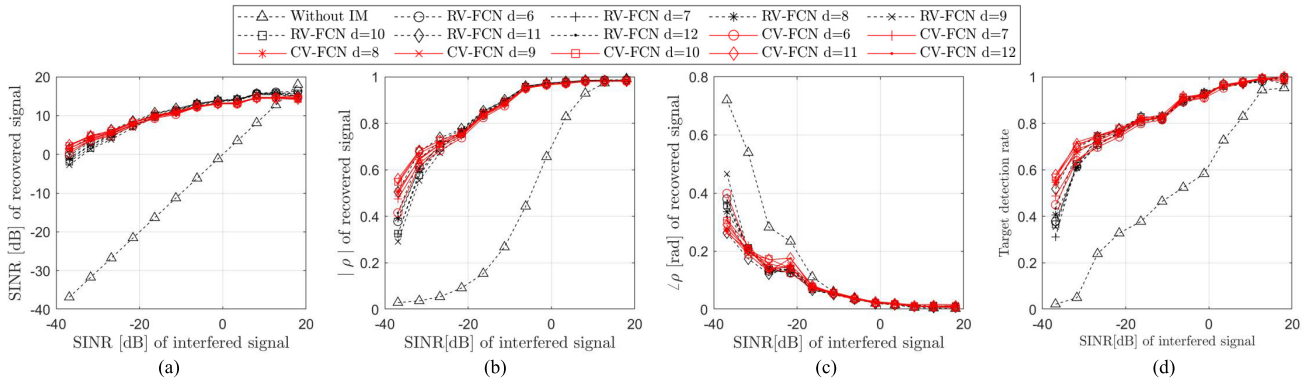

Fig. 9. Performance comparison of the CV-FCNs with the corresponding RV-FCNs in terms of (a) average SINR, (b) modulus, and (c) phase of the correlation coefficient, and (d) target detection rate, where d means the number of convolutional layers in the network.

TABLE IV
COMPARISON OF THE CV-FCN WITH RV-FCN

Method	No. of filters	Depth	Total parameter	SINR (dB) in low SINR scenarios[1]	$\lvert\rho\rvert$ in low SINR scenarios	$\angle\rho$ [rad] in low SINR scenarios	detection rate in low SINR scenarios
CV-FCN	16	6	19170	**3.9687**	**0.6129**	0.2177	**0.6320**
		7	23810	**4.3370**	**0.6364**	**0.2036**	**0.6480**
		8	28450	**4.6703**	**0.6531**	**0.1920**	**0.6783**
		9	33090	**4.8899**	**0.6519**	**0.1911**	**0.6739**
		10	37730	**5.3700**	**0.6786**	**0.2020**	**0.6982**
		11	**42370**	**5.4120(optimal)**	**0.6818**	0.2103	**0.6994**
		12	47010	**5.2010**	**0.6719**	**0.1915**	**0.7010**
RV-FCN	32	6	38178	3.9395	0.6117	**0.2115**	0.6149
		7	47426	3.2449	0.5928	0.2127	0.6026
		8	56674	3.6104	0.6183	0.2037	0.6318
		9	65922	2.3263	0.5683	0.2353	0.6086
		10	75170	2.9225	0.5901	0.2080	0.6251
		11	84418	5.1908(optimal)	0.6744	**0.1744**	0.6826
		12	93666	4.4984	0.6394	0.1945	0.6533

[1] The SINR of interfered signals is between -40 dB and -20 dB.

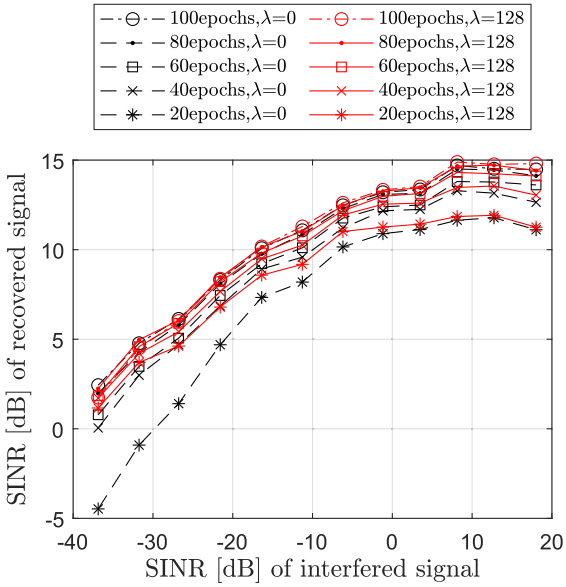

Fig. 10. Performance comparison of CV-FCNs trained with prior-guided loss function using the full dataset (4320 samples) for different epochs.

$\lambda = 0$ (i.e., mse) and $\lambda = 128$ were used in the loss function (6) to illustrate its performance. For both cases, the CV-FCNs were trained for certain epochs varying from 20 to 100 with increasing steps of 20.

The performance of the CV-FCN improves with the increase of training epochs for both cases of $\lambda = 0$ and $\lambda = 128$, as shown in Fig. 10. Meanwhile, a marginal difference between the training results of 80 and 100 epochs shows that the CV-FCNs obtained in both cases converged to a certain suboptimal solution when trained for 100 epochs. However, by introducing the prior feature as a regularization term (e.g., $\lambda = 128$), the features needed for IM can be extracted faster by training and the CV-FCN after only 20 training epochs reaches almost comparable results as that after 100 training epochs, especially in the low SINR scenarios (Fig. 10). By contrast, in the high SINR scenarios, the interference components are relatively small compared to the targets' signals, and noise becomes the dominant disturbance to the signal. Consequently, the mse term becomes the dominant part in the prior-guided loss function and the regularization impact of $L_{2,1}$ norm becomes weaker when λ takes a fixed medium value (e.g., $\lambda = 128$). As a result, it leads to slower training convergence in the high SINR scenarios. To overcome this problem, one possible solution is to adjust the value of λ according to the SNR, which would be considered in the future.

2) Effect on the Size of Training Dataset: To evaluate the effect of prior knowledge incorporation in the loss function on the size of the dataset required for training, we randomly chose $1/2$, $1/4$, and $1/8$ of samples from the training dataset

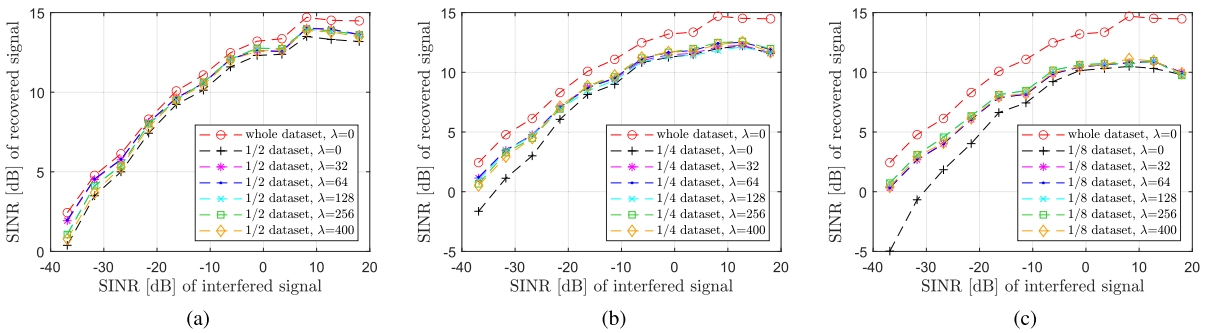

Fig. 11. Performance comparison of CV-FCNs trained with prior-guided loss function using datasets of different sizes. (a) 1/2 of the full dataset (2160 samples). (b) 1/4 of the full dataset (1080 samples). (c) 1/8 of the full dataset (540 samples).

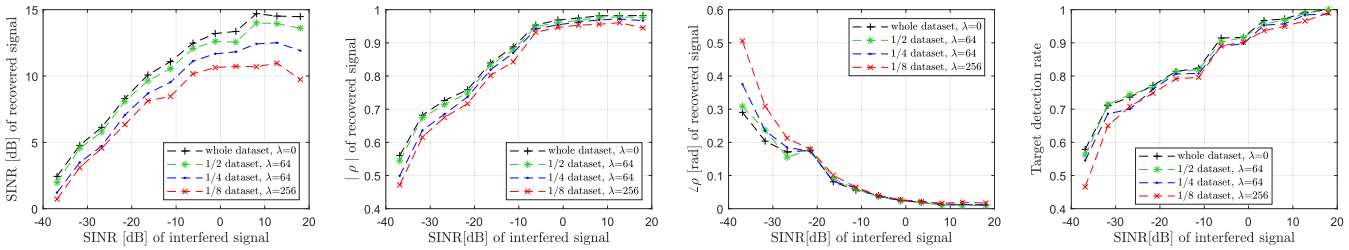

Fig. 12. Performance of CV-FCNs trained with prior-guided loss function using smaller datasets compared to that trained with mse using the full dataset in terms of (a) average SINR, (b) modulus, and (c) phase of the correlation coefficient, and (d) target detection rate.

in Section V-D1 to form three smaller datasets and then used them for the designed CV-FCN (Model A) training. Based on the convergence analysis in Section V-D1, the number of the training epochs was set to 100.

Fig. 11 shows the performance of the CV-FCNs trained using the datasets of different sizes when λ takes various values. The SINRs of recovered signals generally degrade with the shrinkage of training datasets [Fig. 11(a)–(c)]. The smaller the training dataset used compared to the full dataset, the severer the SINR degradation. However, with the increase of λ, the SINRs of recovered signals improve, which are more noticeable in the low SINR scenarios and in a smaller training dataset case. Besides, the CV-FCNs trained with 1/2 or 1/4 of the full data obtained the best results when $\lambda = 64$, while the ones trained with 1/8 of the full data show the highest SINR when $\lambda = 256$. This is because there are more residual interferences in the recovered signals processed by the NNs trained using a smaller dataset; in such situations, the prior feature plays a greater role in suppressing the interference. Note that a larger value of λ (e.g., $\lambda = 400$) may result in the loss of targets' signals when the interference is almost completely removed.

To facilitate the comparison of the regularization effect of the prior knowledge on the size of training dataset, the SINRs, correlation coefficients, and the detection rates of recovered signals with $\lambda = 64$ in Fig. 11(a) and (b) and $\lambda = 256$ in Fig. 11(c) are replotted together in Fig. 12. It is clear that reducing the size of the training dataset results in performance degradation over a wide range of SINRs of input signals. However, with the additional prior information offered by the $L_{2,1}$ norm, the CV-FCNs trained on smaller datasets achieve comparable performance as that on the full dataset in the low SINR scenarios, even when the training dataset is reduced to one eighth. This is because with a small training dataset, the features extracted by the network with mse would be insufficient for IM; thus, the network's performance would worsen. Incorporating the prior information offered by $L_{2,1}$ norm is helpful to guide and improve the features extracted for IM, compensating for the effect of data shortage. Therefore, the proposed IM approach is attractive for small data learning by introducing prior knowledge.

Then, we demonstrate the IM performance of CV-FCNs trained with prior-guided loss function using 1/8 of the full data (i.e., 540 samples). Fig. 13 shows the IM results of an interfered beat signal of three point targets at the distance of 1, 3, and 4 km. Due to strong interferences, the weak target is almost immersed in the raised noise floor [see Fig. 13(a) and (b)]. After being processed with the RV-FCN and CV-FCN obtained with $\lambda = 0$, the interferences and noise are significantly suppressed, and the CV-FCN shows a better performance. However, some residual interference components are still observed [Fig. 13(c)–(f)]. With the increase of λ, the residual interferences and noise are further mitigated [Fig. 13(g)–(k)], and consequently, the noise floor of the range profile decreases as well [Fig. 13(i)]. Besides, it should be noted that the signal loss exists due to limited training data [see Fig. 13(f)–(k)] and it is difficult to handle for the existing DL-based IM approaches with one end-to-end neural network. Furthermore, we would consider introducing a constraint of signal continuity to reduce the loss.

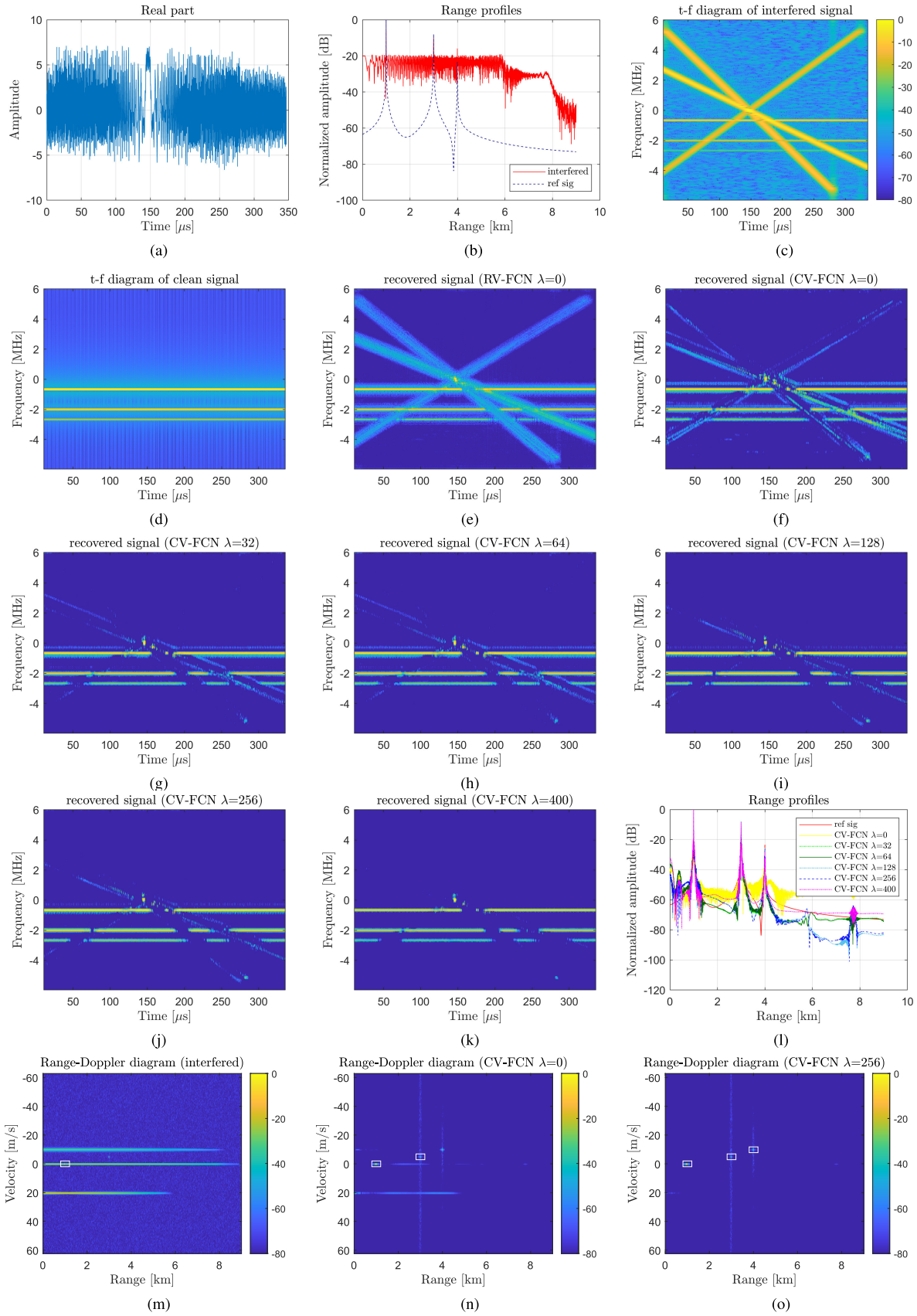

Fig. 13. IM for the simulated radar signal whose SINR is -10.2 dB and SNR is 20 dB. (a) Acquired beat signal contaminated by mutual interferences, (b) its range profiles, (c) its $t-f$ diagram, and (m) its RD map. (d) Interference-free reference. (e) Result of IM of RV-FCN trained with mse using 1/8 of the full data. (f)–(k) Results of IM of CV-FCNs trained with prior-guided loss function using 1/8 of the full data. (l) Corresponding range profiles obtained after IM. (n) and (o) RD maps and its target detection results (white rectangles) of recovered beat signals processed by the CV-FCNs obtained with $\lambda = 0$ and $\lambda = 256$, respectively.

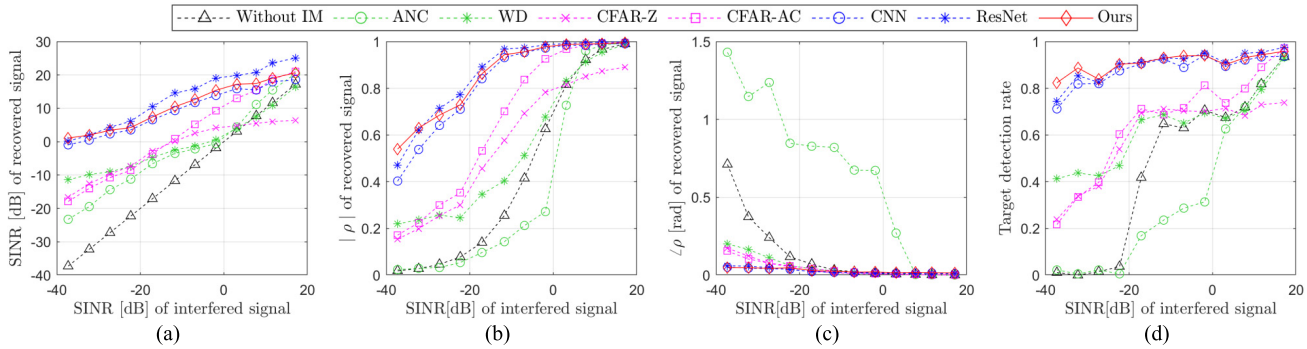

Fig. 14. Performance comparison of our proposed approach with state-of-the-art IM techniques in terms of (a) average SINR, (b) modulus, and (c) phase of the correlation coefficient, and (d) target detection rate.

To further evaluate the performance of the proposed prior-guided IM approach on range-Doppler processing, the beat signals in the 256 consecutive sweeps were generated for the scenario above with three point targets at 1, 3, and 4 km. The targets' Doppler velocities were set to 0, -5, and -10 m/s relative to the primary radar, and three aggressor FMCW radars moved away from the primary radar with Doppler velocities of 0, -10, and 20 m/s. The RD map of the interfered beat signal is shown in Fig. 13(m). The white rectangle represents the point if the detector labels it as a target. Due to the strong interferences, the two targets at the distance of 3 and 4 km cannot be detected. Then, the CV-FCNs trained with prior-guided loss function using 1/8 of the full data are used to process the radar data in a frame. For conciseness, only the RD maps of recovered beat signals obtained with $\lambda = 0$ and $\lambda = 256$ are given in Fig. 13(n) and (o). After IM with $\lambda = 0$, although most interferences and noise are suppressed, some residual interference components exist and the target at the distance of 4 km still cannot be distinguished [Fig. 13(n)]. With the value of λ increased to 256, the interferences are further mitigated, and all the targets can be accurately detected in the RD map, as shown in Fig. 13(o).

Therefore, by tuning the hyperparameter λ, the prior information characterized by $L_{2,1}$ norm can enforce the CV-FCN to extract meaningful features for IM faster during training, thus accelerating the convergence rate of training. Moreover, by incorporating the prior information, the proposed CV-FCNs can be trained with a smaller dataset, which is attractive for IM problems as it is generally very difficult to acquire labeled real radar data in practice, especially for dynamic scenarios.

E. Comparative Analysis With Other IM Techniques

The performance of our proposed approach is compared with that of several state-of-the-art IM methods, including traditional signal processing approaches, i.e., the wavelet denoising (WD)-based method [8], adaptive noise canceller (ANC) [7], CFAR-Z and CFAR-AC [4], and DL-based approaches, i.e., CNN-based method [14] and ResNet-based method [24]. The parameters used in the aforementioned traditional signal processing approaches are listed in Table V, which were tuned to achieve the optimal performance in the synthetic dataset. The CV-FCN was trained with prior-guided loss function where $\lambda = 128$ and the CNN and ResNet were trained with the mse. We used the simulated radar signals for test and quantitatively evaluated the performance of different methods.

TABLE V
PARAMETERS IN THE SELECTED TRADITIONAL SIGNAL PROCESSING APPROACHES FOR COMPARISON

Method	Parameter	Value
CFAR-Z/AC	Number of Training Cells	450
	Number of Guard Cells	150
	Probability of False Alarm	0.001
	Dilation size	18
WD	Level of wavelet decomposition	9
ANC	Interference power threshold	20% signal power
	Filter length	170
	Fraction of the upper bond of step size	1.9

The SINRs, correlation coefficients, and the detection rates of the obtained signals after IM with different approaches are shown in Fig. 14. Our proposed IM approach based on prior-guided CV-FCN generally performs better than the other methods. Although the ResNet-based approach achieves comparable performance as the proposed one, it has 29$\times$ more parameters than the proposed CV-FCN, which would lead to memory burden and much higher computation complexity.

On the other hand, the CFAR-Z and CFAR-AC use CFAR to detect the interference components of acquired beat signals in the $t-f$ spectrum. The detection accuracy is determined by the selected parameters. Then CFAR-Z uses zeroing to mitigate detected interferences, which naturally removes targets' beat signals at the same time. Different from CFAR-Z, CFAR-AC uses AC to reconstruct the beat signals removed by zeroing, which shows better performance than CFAR-Z, especially in high SINR scenarios. Besides, a WD-based method can reconstruct and remove the interferences in the wavelet domain, which shows a good performance in low SINR scenarios. In the ANC method, the negative half of the FFT spectrum is used as the input of its reference channel, and the threshold needs to be manually adjusted for different levels of interference. As the positive and negative parts are not ideally conjugate symmetric as assumed in [7], the IM

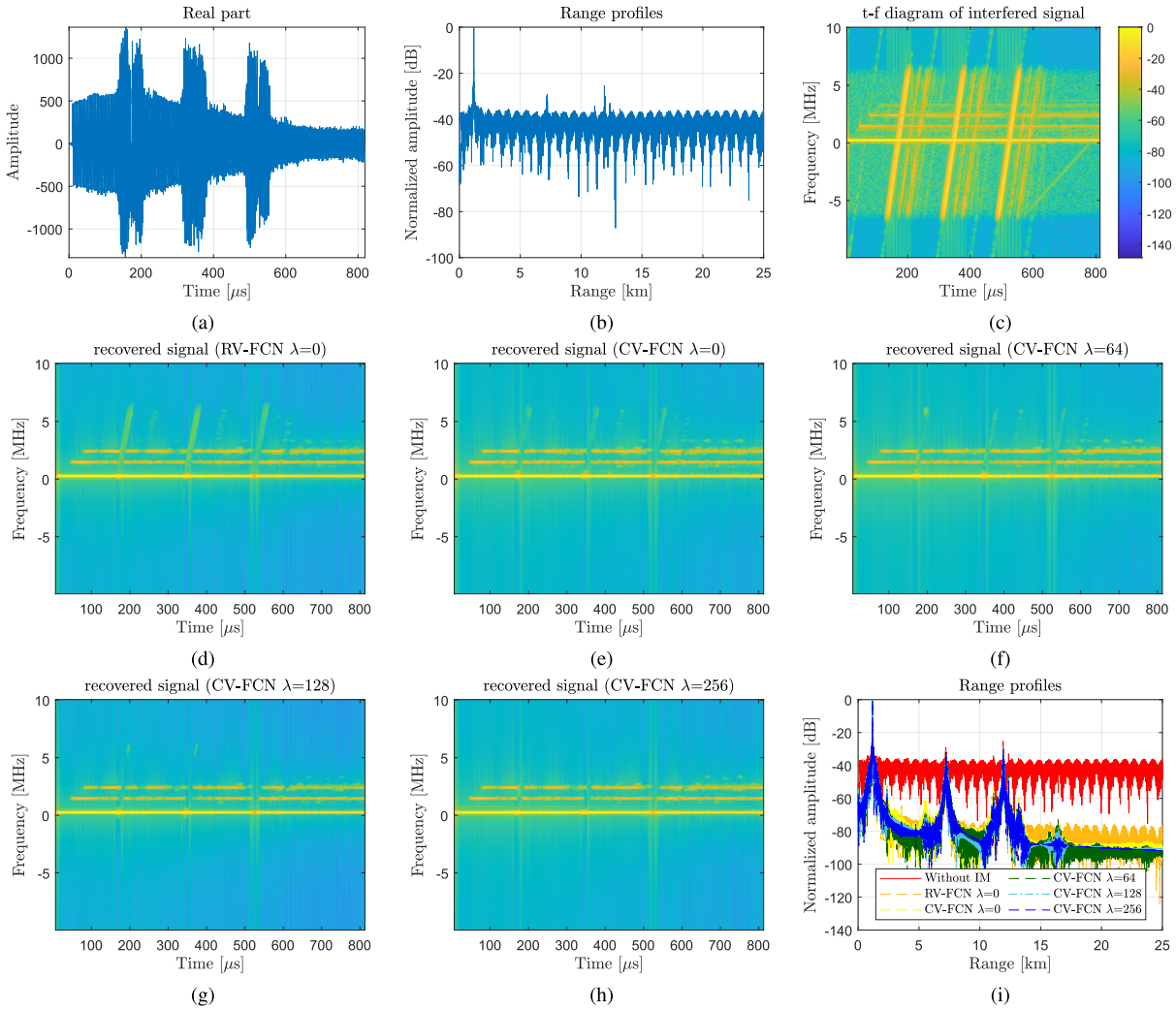

Fig. 15. IM for measured radar signals in the scene of the industrial chimney and surrounding buildings. (a) Acquired beat signal contaminated by mutual interferences, (b) its range profiles, and (c) its $t-f$ diagram. (d) Results of IM of the RV-FCN trained with mse. (e)–(h) Results of IM of the CV-FCNs trained with prior-guided loss function. (i) Corresponding range profiles obtained after IM. All the models were trained using only simulated data.

performance of the ANC would degrade, resulting in a correlation coefficient with lower modulus and higher argument, as shown in Fig. 14(b) and (c). As described, the performance of the above traditional signal processing methods depends on a proper selection of a few manually adjustable parameters. Over a wide range of the SINR variations, their performance is not as good as the selected DL-based methods.[1]

VI. Measuremnt Results

The measured radar signals collected as described in Section IV-B are used to verify the generalization of the proposed IM approach.

For conciseness, we analyze the IM performance in the scene of the industrial chimney and surrounding buildings. As the clean reference signals are unavailable, the quantitative evaluation of the IM performance is omitted here. Instead, the qualitative results, including the signal waveforms in the time domain, the $t-f$ diagrams, and the range profiles, are shown in Fig. 15. In Fig. 15(a), three large pulses can be observed in the received radar signal, which is caused by the strong interferences. The interference-contaminated beat signal leads to a range profile with significantly increased noise floor, and the two weaker targets are almost overwhelmed [see Fig. 15(b)]. Using the STFT algorithm with the same parameter setting as for the simulated signals, the $t-f$ spectrum of the beat signal is computed [Fig. 15(c)], where three inclined thick lines represent the interferences.

To suppress the interferences, the RV-FCN and CV-FCN obtained in Section V-B are used. Note the networks were trained using only the synthetic radar dataset and the prior-guided loss function.

The $t-f$ maps of the recovered signal processed by the RV-FCN and CV-FCN are shown in Fig. 15(d) and (e). With the RV-FCN, the interferences are entirely removed in the negative frequency, but some residuals are still observed in the positive frequency spectrum [Fig. 15(d)].

[1]In principle, the range of SINRs of input signals can be divided into a few smaller intervals. By tuning the related parameters of conventional methods over each interval, they could outperform the DL-based methods. However, selecting such a set of parameters is nontrivial in practice.

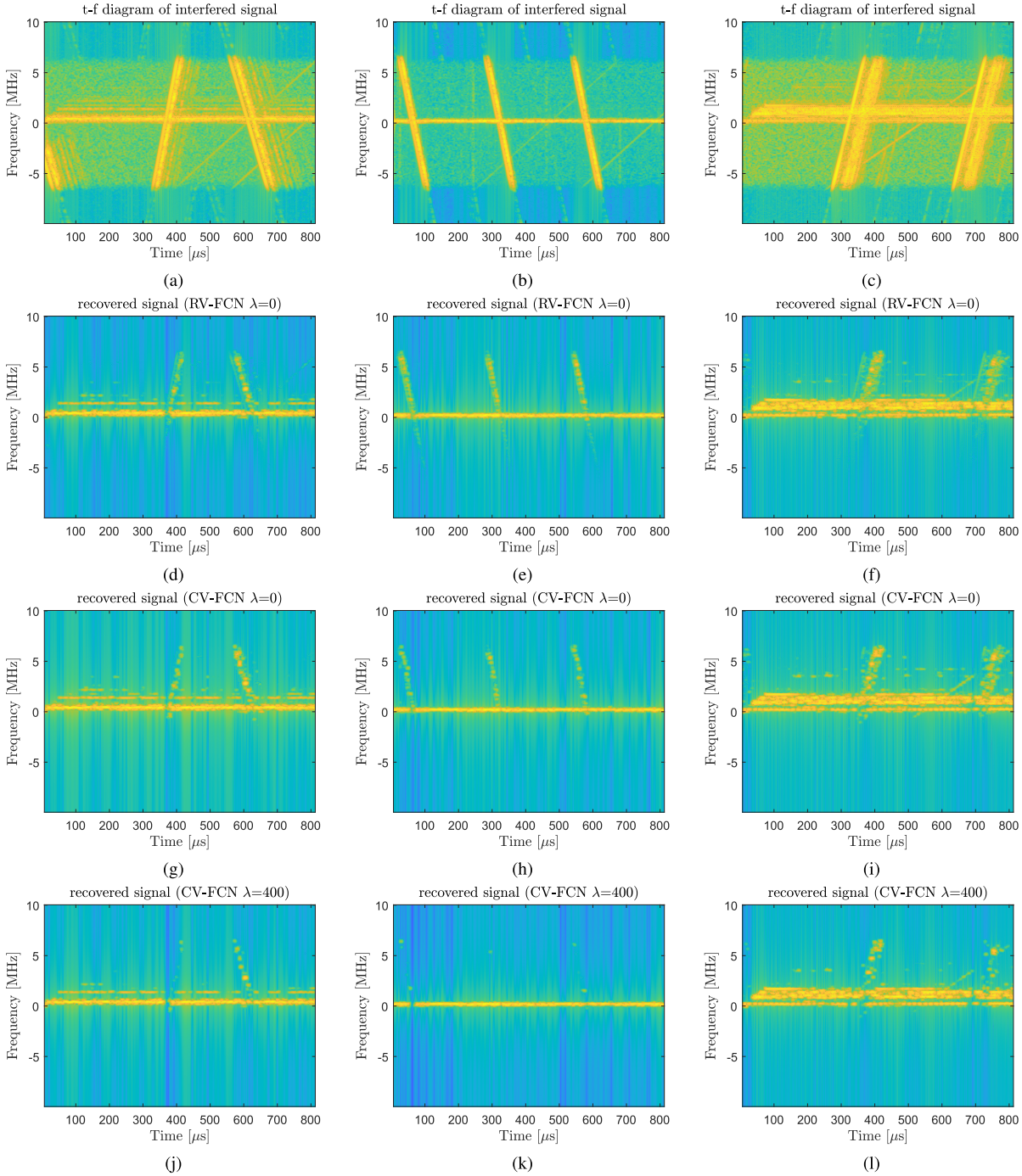

Fig. 16. IM for measured radar signals in three scenarios (A13 highway with traffic flow in Delft, a street with moving cars, and a rotating wind turbine from left to right). (a)–(c) $t-f$ diagrams of acquired beat signals contaminated by mutual interferences. (d)–(f) Results of IM of the RV-FCN trained with mse. (g)–(i) Results of IM of the CV-FCN trained with mse. (j)–(l) Results of IM of the CV-FCN trained with prior-guided loss function where λ is 400.

In contrast, a better IM performance is achieved with the CV-FCN [see Fig. 15(e)]. This shows a better generalization performance of the CV-FCN, compared to that of the RV-FCN, in the experimental data although it was trained with only the synthetic radar dataset. Moreover, with the increase of the value of λ, the residual interference components and noise are further suppressed [as shown in Fig. 15(e)–(h)]. After IM, three peaks of targets can be clearly seen in the range profiles in Fig. 15(i), and the CV-FCN results in a lower noise floor than the RV-FCN, which would be of benefit to improve the detection probability of targets.

The RV-FCN and the proposed CV-FCN were also used to mitigate interference for the measured radar signals collected in the other three scenes: A13 highway with traffic flow in Delft, a street with traffic flow, and a rotating wind turbine. The processing results for three examples are shown in the three columns in Fig. 16. From Fig. 16(d) to (i), the CV-FCN achieves slightly better IM performance than the RV-FCN

when $\lambda = 0$, but some residual interferences still can be seen in the $t-f$ spectrograms obtained with both approaches. By increasing λ, the proposed CV-FCN significantly suppresses the interferences and noise [see Fig. 16(j)–(l)], and the desired targets' spectra are recovered.

The experimental results on measured radar signals collected in various real-world scenes have shown a better generalization performance of the proposed CV-FCN. Moreover, these experiments also validate that incorporating prior feature constraints in the loss function for training of the CV-FCN is helpful to suppress the interferences and noise in measured radar signals. Therefore, the proposed prior-guided CV-FCN-based IM approach can be readily applied in reality.

VII. Conclusion

In this article, a prior-guided DL-based IM approach has been proposed for FMCW radars. The prior expert feature is introduced as a regularization term in the loss function for the neural network training. The experimental results show that the proposed CV-FCN-based IM approach, compared to the existing traditional and DL-based IM techniques, achieves the state-of-the-art performance in terms of the SINRs, correlation coefficient, and the detection rate of recovered signals. Moreover, the use of the prior-guided loss function significantly accelerates the training of the proposed CV-FCN and reduces the size of required training dataset. Furthermore, the experimental results with measured data demonstrate that the generalization performance of the proposed CV-FCN-based IM approach greatly improves by incorporating prior features even if it was trained with only synthetic radar data. These merits make the proposed CV-FCN-based IM approach to be readily applied in practice. Finally, to further optimize the proposed network architecture and training procedure, designing an optimization algorithm to automatically tune the hyperparameter λ in the prior-guided loss function is necessary and will be considered in the future.

Acknowledgment

The authors would like to thank F. van der Zwan from TU Delft, Delft, The Netherlands, for his help with experimental measurements and for providing the data.

References

[1] M. Rameez, M. Dahl, and M. I. Pettersson, "Autoregressive model-based signal reconstruction for automotive radar interference mitigation," *IEEE Sensors J.*, vol. 21, no. 5, pp. 6575–6586, Mar. 2021.

[2] F. Uysal, "Phase-coded FMCW automotive radar: System design and interference mitigation," *IEEE Trans. Veh. Technol.*, vol. 69, no. 1, pp. 270–281, Jan. 2020.

[3] J. Bechter, F. Roos, M. Rahman, and C. Waldschmidt, "Automotive radar interference mitigation using a sparse sampling approach," in *Proc. Eur. Radar Conf. (EURAD)*, Oct. 2017, pp. 90–93.

[4] J. Wang, "CFAR-based interference mitigation for FMCW automotive radar systems," *IEEE Trans. Intell. Transp. Syst.*, vol. 23, no. 8, pp. 12229–12238, Aug. 2022.

[5] J. Wang, M. Ding, and A. Yarovoy, "Matrix-pencil approach-based interference mitigation for FMCW radar systems," *IEEE Trans. Microw. Theory Techn.*, vol. 69, no. 11, pp. 5099–5115, Nov. 2021.

[6] J. Bechter, K. D. Biswas, and C. Waldschmidt, "Estimation and cancellation of interferences in automotive radar signals," in *Proc. 18th Int. Radar Symp. (IRS)*, Jun. 2017, pp. 1–10.

[7] F. Jin and S. Cao, "Automotive radar interference mitigation using adaptive noise canceller," *IEEE Trans. Veh. Technol.*, vol. 68, no. 4, pp. 3747–3754, Apr. 2019.

[8] S. Lee, J.-Y. Lee, and S.-C. Kim, "Mutual interference suppression using wavelet denoising in automotive FMCW radar systems," *IEEE Trans. Intell. Transp. Syst.*, vol. 22, no. 2, pp. 887–897, Feb. 2021.

[9] M. Wagner, F. Sulejmani, A. Melzer, P. Meissner, and M. Huemer, "Threshold-free interference cancellation method for automotive FMCW radar systems," in *Proc. IEEE Int. Symp. Circuits Syst. (ISCAS)*, May 2018, pp. 1–4.

[10] T. Fei, H. Guang, Y. Sun, C. Grimm, and E. Warsitz, "An efficient sparse sensing based interference mitigation approach for automotive radar," in *Proc. 17th Eur. Radar Conf. (EuRAD)*, Jan. 2021, pp. 274–277.

[11] Z. Xu and M. Yuan, "An interference mitigation technique for automotive millimeter wave radars in the tunable Q-factor wavelet transform domain," *IEEE Trans. Microw. Theory Techn.*, vol. 69, no. 12, pp. 5270–5283, Dec. 2021.

[12] J. Bechter, K. Eid, F. Roos, and C. Waldschmidt, "Digital beamforming to mitigate automotive radar interference," in *IEEE MTT-S Int. Microw. Symp. Dig.*, May 2016, pp. 1–4.

[13] X. Li, Y. He, and X. Jing, "A survey of deep learning-based human activity recognition in radar," *Remote Sens.*, vol. 11, no. 9, p. 1068, Jan. 2019.

[14] J. Rock, M. Toth, E. Messner, P. Meissner, and F. Pernkopf, "Complex signal denoising and interference mitigation for automotive radar using convolutional neural networks," in *Proc. 22th Int. Conf. Inf. Fusion (FUSION)*, Jul. 2019, pp. 1–8.

[15] J. Rock, M. Toth, P. Meissner, and F. Pernkopf, "Deep interference mitigation and denoising of real-world FMCW radar signals," in *Proc. IEEE Int. Radar Conf. (RADAR)*, Apr. 2020, pp. 624–629.

[16] J. Rock, W. Roth, M. Toth, P. Meissner, and F. Pernkopf, "Resource-efficient deep neural networks for automotive radar interference mitigation," *IEEE J. Sel. Topics Signal Process.*, vol. 15, no. 4, pp. 927–940, Jun. 2021.

[17] N.-C. Ristea, A. Anghel, and R. Tudor Ionescu, "Fully convolutional neural networks for automotive radar interference mitigation," 2020, *arXiv:2007.11102*.

[18] M. L. L. de Oliveira and M. J. G. Bekooij, "Deep convolutional autoencoder applied for noise reduction in range-Doppler maps of FMCW radars," in *Proc. IEEE Int. Radar Conf. (RADAR)*, Apr. 2020, pp. 630–635.

[19] S. Chen, J. Taghia, T. Fei, U. Kuhnau, N. Pohl, and R. Martin, "A DNN autoencoder for automotive radar interference mitigation," in *Proc. IEEE Int. Conf. Acoust., Speech Signal Process. (ICASSP)*, Jun. 2021, pp. 4065–4069.

[20] J. Fuchs, A. Dubey, M. Lubke, R. Weigel, and F. Lurz, "Automotive radar interference mitigation using a convolutional autoencoder," in *Proc. IEEE Int. Radar Conf. (RADAR)*, Apr. 2020, pp. 315–320.

[21] C. Jiang, T. Chen, and B. Yang, "Adversarial interference mitigation for automotive radar," in *Proc. IEEE Radar Conf. (RadarConf21)*, May 2021, pp. 1–6.

[22] J. Mun, H. Kim, and J. Lee, "A deep learning approach for automotive radar interference mitigation," in *Proc. IEEE 88th Veh. Technol. Conf. (VTC-Fall)*, Aug. 2018, pp. 1–5.

[23] J. Mun, S. Ha, and J. Lee, "Automotive radar signal interference mitigation using RNN with self attention," in *Proc. IEEE Int. Conf. Acoust., Speech Signal Process. (ICASSP)*, May 2020, pp. 3802–3806.

[24] W. Fan et al., "Interference mitigation for synthetic aperture radar based on deep residual network," *Remote Sens.*, vol. 11, no. 14, p. 1654, Jul. 2019.

[25] S. Chen, W. Shangguan, J. Taghia, U. Kuhnau, and R. Martin, "Automotive radar interference mitigation based on a generative adversarial network," in *Proc. IEEE Asia–Pacific Microw. Conf. (APMC)*, Dec. 2020, pp. 728–730.

[26] N.-C. Ristea, A. Anghel, R. T. Ionescu, and Y. C. Eldar, "Automotive radar interference mitigation with unfolded robust PCA based on residual overcomplete auto-encoder blocks," in *Proc. IEEE/CVF Conf. Comput. Vis. Pattern Recognit. Workshops (CVPRW)*, Jun. 2021, pp. 3203–3208.

[27] D. A. Brooks, O. Schwander, F. Barbaresco, J.-Y. Schneider, and M. Cord, "Complex-valued neural networks for fully-temporal micro-Doppler classification," in *Proc. 20th Int. Radar Symp. (IRS)*, Jun. 2019, pp. 1–10.

[28] P. Virtue, S. X. Yu, and M. Lustig, "Better than real: Complex-valued neural nets for MRI fingerprinting," in *Proc. IEEE Int. Conf. Image Process. (ICIP)*, Sep. 2017, pp. 3953–3957.

[29] Y. Arima and A. Hirose, "Millimeter-wave coherent imaging of moving targets by using complex-valued self-organizing map and autoencoder," *IEEE J. Sel. Topics Appl. Earth Observ. Remote Sens.*, vol. 13, pp. 1784–1797, 2020.
[30] C. Trabelsi et al., "Deep complex networks," 2017, *arXiv:1705.09792*.
[31] A. Hirose and S. Yoshida, "Generalization characteristics of complex-valued feedforward neural networks in relation to signal coherence," *IEEE Trans. Neural Netw. Learn. Syst.*, vol. 23, no. 4, pp. 541–551, Apr. 2012.
[32] M. Abadi et al., "TensorFlow: A system for large-scale machine learning," in *Proc. 12th USENIX Symp. Operating Syst. Design Implement. (OSDI)*, 2016, pp. 265–283.
[33] M. Arjovsky, A. Shah, and Y. Bengio, "Unitary evolution recurrent neural networks," in *Proc. 33rd Int. Conf. Mach. Learn.*, 2016, pp. 1120–1128.
[34] N. Guberman, "On complex valued convolutional neural networks," 2016, *arXiv:1602.09046*.
[35] B. G. Bodmann and P. K. Singh, "Burst erasures and the mean-square error for cyclic Parseval frames," *IEEE Trans. Inf. Theory*, vol. 57, no. 7, pp. 4622–4635, Jul. 2011.
[36] X. Gao, S. Roy, and G. Xing, "MIMO-SAR: A hierarchical high-resolution imaging algorithm for mmWave FMCW radar in autonomous driving," *IEEE Trans. Veh. Technol.*, vol. 70, no. 8, pp. 7322–7334, Aug. 2021.
[37] K. Simonyan and A. Zisserman, "Very deep convolutional networks for large-scale image recognition," 2014, *arXiv:1409.1556*.
[38] Y. Jiang, H. Li, and M. Rangaswamy, "Deep learning denoising based line spectral estimation," *IEEE Signal Process. Lett.*, vol. 26, no. 11, pp. 1573–1577, Nov. 2019.
[39] K. He, X. Zhang, S. Ren, and J. Sun, "Deep residual learning for image recognition," in *Proc. IEEE Conf. Comput. Vis. Pattern Recognit. (CVPR)*, Jun. 2016, pp. 770–778.

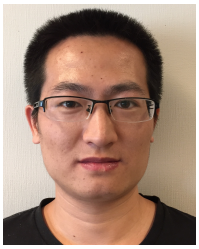

Jianping Wang (Member, IEEE) received the Ph.D. degree in electrical engineering from the Delft University of Technology, Delft, The Netherlands, in 2018.

From August 2012 to April 2013, he worked as a Research Associate with the University of New South Wales, Sydney, NSW, Australia, on frequency-modulated continuous-wave synthetic aperture radar signal processing for formation flying satellites. He is currently a Post-Doctoral Researcher with the Group of Microwave Sensing, Signals and Systems (MS3), Delft University of Technology. His research interests include microwave imaging, signal processing, and antenna array design.

Dr. Wang was a TPC Member of the IET International Radar Conference, Nanjing, China, in 2018. He was a Finalist of the Best Student Paper Awards in the International Workshop on Advanced Ground Penetrating Radar (IWAGPR), Edinburgh, U.K., in 2017, and the International Conference on Radar, Brisbane, QLD, Australia, in 2018. He has served as a reviewer for many IEEE journals.

Runlong Li received the B.S. degree from the Beijing University of Posts and Telecommunications, Beijing, China, in 2020. He is currently pursuing the M.S. degree in information and communication engineering with the Beijing University of Posts and Telecommunications.

His research interests include radar signal processing, deep learning, and autonomous driving.

Yuan He (Senior Member, IEEE) received the B.Sc. and M.Sc. degrees from the National University of Defense Technology, Changsha, China, in 2007 and 2010, respectively, and the Ph.D. degree from the Delft University of Technology, Delft, The Netherlands, in 2014.

He is currently an Associate Professor with the Beijing University of Posts and Telecommunications, Beijing, China. His main research interests are radar signal processing, wireless communication, and electromagnetic computation.

Yang Yang (Member, IEEE) received the Ph.D. degree from Tianjin University, Tianjin, China, in 2019.

He is currently an Assistant Professor with Tianjin University. His research interests include deep learning, pattern recognition, object detection, human activity recognition, and micro-Doppler radar.